Systems/Circuits

Parallel Pathways Provide Hippocampal Spatial Information to Prefrontal Cortex

Kokoe Fany Messanvi, Kathleen Berkun, Aster Perkins, and Yogita Chudasama
Section on Behavioral Neuroscience, National Institute of Mental Health, National Institutes of Health, Bethesda, Maryland 20892

Long-range synaptic connections define how information flows through neuronal networks. Here, we combined retrograde and anterograde trans-synaptic viruses to delineate areas that exert direct and indirect influence over the dorsal and ventral prefrontal cortex (PFC) of the rat (both sexes). Notably, retrograde tracing using pseudorabies virus (PRV) revealed that both dorsal and ventral areas of the PFC receive prominent disynaptic input from the dorsal CA3 (dCA3) region of the hippocampus. The PRV experiments also identified candidate anatomical relays for this disynaptic pathway, namely, the ventral hippocampus, lateral septum, thalamus, amygdala, and basal forebrain. To determine the viability of each of these relays, we performed three additional experiments. In the first, we injected the retrograde monosynaptic tracer Fluoro-Gold into the PFC and the anterograde monosynaptic tracer Fluoro-Ruby into the dCA3 to confirm the first-order connecting areas and revealed several potential relay regions between the PFC and dCA3. In the second, we combined PRV injection in the PFC with polysynaptic anterograde viral tracer (HSV-1) in the dCA3 to reveal colabeled connecting neurons, which were evident only in the ventral hippocampus. In the third, we combined retrograde adeno-associated virus (AAV) injections in the PFC with an anterograde AAV in the dCA3 to reveal anatomical relay neurons in the ventral hippocampus and dorsal lateral septum. Together, these findings reveal parallel disynaptic pathways from the dCA3 to the PFC, illuminating a new anatomical framework for understanding hippocampal–prefrontal interactions. We suggest that the representation of context and space may be a universal feature of prefrontal function.

Key words: **CA3; dorsal hippocampus; prefrontal function; rat; viral tracing; relays**

Significance Statement

The known functions of the prefrontal cortex are shaped by input from multiple brain areas. We used transneuronal viral tracing to discover multiple prominent disynaptic pathways through which the dorsal hippocampus (specifically, the dorsal CA3) has the potential to shape the actions of the prefrontal cortex. The demonstration of neuronal relays in the ventral hippocampus and lateral septum presents a new foundation for understanding long-range influences over prefrontal interactions, including the specific contribution of the dorsal CA3 to prefrontal function.

Introduction

Knowledge of the synaptic influences over prefrontal circuitry is foundational for understanding its role in behavior and disease (Chudasama and Robbins, 2006). Much of our understanding about prefrontal afference stems from conventional retrograde tracers (Barbas and Blatt, 1995; Hoover and Vertes, 2007; Bedwell et al., 2014), which reveal inputs from cortical and subcortical brain regions that contribute to a wide range of functions. The projections demonstrated from the thalamus, hippocampus, and amygdala are thought to shape normal prefrontal function, a prediction borne out by the behavioral deficits that arise by studies applying interhemispheric disconnection lesions between the prefrontal cortex (PFC) and each of these areas (Churchwell et al., 2009; Chudasama et al., 2012; Browning et al., 2015). Less clear however, is the influence of areas that project to the prefrontal cortex through a synaptic relay. These upstream areas, just one synapse removed, greatly expand the sphere of potential influence over prefrontal function. Here, we use neurotropic viral tracers to

Received Apr. 29, 2022; revised Oct. 6, 2022; accepted Nov. 7, 2022.

Author contributions: K.F.M. and Y.C. designed research; K.F.M., K.B., and A.P. performed research; K.F.M., K.B., A.P., and Y.C. analyzed data; K.F.M. and Y.C. wrote the paper.

This work was supported by Intramural Research Program of the National Institute of Mental Health (NIMH) Grants ZIA MH002951 and ZIC MH002952 to Y.C. We thank NIMH Systems Neuroscience Imaging Resource for help with image acquisition, the NIMH Rodent Behavioral Core for use of the surgery suite, James Shaw and Matthew Gastinger for the training on how to use Imaris software, the Center for Neuroanatomy with Neurotrophic Viruses for providing strains of pseudorabies virus and HSV, and Drs. Edward Boyden at Massachusetts Institute of Technology and James M. Wilson at University of Pennsylvania for the gift of retrograde and anterograde adeno-associated viruses.

K. Berkun's present address: Decibel Therapeutics, Boston, Massachusetts 02215.

A. Perkins's present address: Icahn School of Medicine at Mount Sinai, New York, New York.

The authors declare no competing financial interests.

Correspondence should be addressed to Kokoe Fany Messanvi at kokoefany.messanvi@nih.gov.

https://doi.org/10.1523/JNEUROSCI.0846-22.2022

Table 1. Summary details for intracranial injection sites and viruses for all brain regions

Groups	Injection targets	Stereotaxic coordinates AP/ML/DV (mm)	Virus	Volume	Titer/concentration
Group 1	dPFC	+3.24/±0.6/−1.5	PRV-614	0.4 μl	9.05×10^8 pfu/ml
$n = 12$	vPFC	+3.24/±0.6/−3.5	PRV-152	0.2 μl	1.31 × 10^9 pfu/ml
Group 2	dPFC	+3.24/±0.6−1.5	FG	0.4 μl	4%
$n = 7$	dCA3	−3.96/±4.5/−3.2	FR	0.3 μl	10%
	vPFC	+3.24/±0.6/−3.5	FG	0.4 μl	4%
	dCA3	−3.96/±4.5/−3.2	FR	0.3 μl	10%
Group 3	dPFC	+3.24/±0.6−1.5	PRV-614	0.4 μl	9.05×10^8 pfu/ml
$n = 5$	dCA3	−3.96/±4.5/−3.2	H129-772	0.3 μl	5.9 × 10^8 pfu/ml
	vPFC	+3.24/±0.6/−3.5	PRV-152	0.4 μl	1.31 × 10^9 pfu/ml
	dCA3	−3.96/±4.5/−3.2	H129-373	0.3 μl	4.68 × 10^8 pfu/ml
Group 4	dPFC	+3.24/±0.6−1.5	AAVrg tdTomato	0.1 to 0.3 μl	7 × 10^13 vg/ml
$n = 4$	vPFC	+3.24/±0.6/−3.5	AAVrg-EGFP	0.1 to 0.3 μl	1 × 10^13 vg/ml
	dHC	−3.96/±4.5/−3.2	AAV1-cerulean	0.1 to 0.3 μl	3.5 × 10^13 vg/ml

investigate the sources of disynaptic anatomical input to the prefrontal cortex.

The rodent prefrontal cortex can be conceptually divided into two major divisions, dorsal and ventral. These subdivisions are associated with distinct anatomical connections (Heidbreder and Groenewegen, 2003; Hoover and Vertes, 2007; Prasad and Chudasama, 2013), as well as distinct functional roles in cognition (Passetti et al., 2002; Chudasama et al., 2003; Chudasama and Robbins, 2003, 2006). The dorsal prefrontal cortex (dPFC), comprising the anterior cingulate (area Cg1/Cg2) and the dorsal half of the prelimbic cortex (PrL), receives cortical input from sensorimotor areas and the retrosplenial cortex, and subcortical input from the intralaminar nuclei and the mediodorsal thalamus (Berendse and Groenewegen, 1991; Shibata et al., 2004; Alcaraz et al., 2016; Bedwell and Tinsley, 2018). Accordingly, lesions centered on the dPFC in rats impair spatial learning and memory (Cholvin et al., 2016), temporal ordering and motor sequencing (Delatour and Gisquet-Verrier, 2001; Chiba et al., 1994), and the normal control of visuospatial attention (Chudasama et al., 2003, 2005; Chudasama and Robbins, 2004; Kim et al., 2016; Luchicchi et al., 2016). In contrast, the ventral prefrontal cortex (vPFC), which groups the ventral portion of the PrL, the infralimbic cortex (IL), and the orbitofrontal cortex, is densely innervated by core limbic regions, namely, the ventral CA1 of the hippocampus and amygdala, as well as the perirhinal cortex and midline thalamus. Lesions to the vPFC affect the normal adaptive control of actions that enable flexibility, including fear expression, decision-making, and response control (Ragozzino et al., 1999; Chudasama and Robbins, 2003; Rudebeck et al., 2006; Eagle et al., 2008; Mar et al., 2011; Kim and Cho, 2017; Moscarello and Maren, 2018).

The actions of the prefrontal cortex are also influenced by indirect projections, although the specific pathways are difficult to study and therefore subject to speculation. However, indirect anatomical pathways can be studied systematically using transsynaptic viruses. For example, in a previous study examining cortical influences over the hippocampus, the prefrontal cortex was found to provide disynaptic input to the hippocampus, whose two longitudinal segments were differentially innervated by distinct prefrontal subregions, with potential relays in the thalamus and entorhinal cortex (Prasad and Chudasama, 2013). In this study, we ask whether disynaptic innervation of the prefrontal cortex might be similarly revealed using multisynaptic anatomical tracers. We report the unexpected finding that the most prominent source of disynaptic innervation to both dorsal and ventral prefrontal subregions is the dorsal CA3 (dCA3) of the hippocampus. The viability of candidate relays was assessed using a combination of anterograde and retrograde viral tracers. We discuss the potential influence of dCA3 over prefrontal function through these disynaptic pathways.

Materials and Methods

Experimental design. We used a combination of anterograde and retrograde trans-synaptic viruses to identify the multisynaptic circuitry associated with the dorsal and ventral PFC of rats. First, we injected a monomeric red fluorescent protein (mRFP)-expressing trans-synaptic pseudorabies virus (PRV-614) and a green fluorescent protein (GFP)-expressing pseudorabies virus (PRV-152) directly into the dPFC and vPFC, respectively. We discovered that the anterior portion of the dCA3 provides disynaptic input to both prefrontal regions via several potential relays, including the ventral hippocampus (vHC), lateral septum, thalamus, amygdala, and basal forebrain. Since disynaptic tracing can be ambiguous with respect to specific relays, subsequent studies were aimed toward confirming the specificity of the synaptic relay. First, we combined retrograde Fluoro-Gold (FG) in the PFC with anterograde Fluoro-Ruby (FR) in dCA3 and examined the brain areas where FG-labeled cell bodies were in the vicinity of FR-labeled terminals and fibers. We then combined PFC injections of retrograde PRV with dCA3 injections of anterograde HSV-1 to identify specific connecting neurons within the potential relay regions. The presence of colabeled cells confirmed connecting links specifically within the vHC only. Finally, we combined retrograde adeno-associated viruses (AAVs) in the dPFC (tdTomato) and vPFC (EGFP), with an anterograde AAV with transsynaptic properties in the dCA3 (cerulean) and confirmed that both vHC and lateral septum were the two connecting relays between the dCA3 and PFC. The different combinations of viral and nonviral injections are reported in Table 1.

Subjects. All experimental procedures were approved by the National Institute of Mental Health Institutional Animal Care and Use Committee, in accordance with the National Institutes of Health (NIH) guidelines for the use of animals. Male and female Long–Evans rats (Envigo) weighing between 250 and 400 g were used for these experiments. Animals were group housed, and water and food were available *ad libitum* under diurnal conditions (12 h light/dark cycle). In accordance with the NIH Department of Occupational Health, Biological Safety and Compliance, injections of PRV and HSV were conducted in a Biosafety Level 2 containment facility.

Viral and conventional tracers. Pseudorabies-Bartha, an attenuated vaccine strain of PRV, has been used for its ability to transport transsynaptically in a retrograde direction (Card et al., 1993; O'Donnell et al., 1997). Several fluorescent recombinants have been developed and validated in the past years (Card and Enquist, 2014). We used the recombinant 152 (expressing GFP) and 614 (expressing mRFP). The H129 strain

of HSV-1 transports trans-synaptically in the anterograde direction (Barnett et al., 1995; Dum et al., 2009). In this study, we used H129-373 (expressing mCherry) and H129-772 (expressing YFP). Both PRV and HSV-1 were obtained from the Center for Neuroanatomy with Neurotrophic Viruses. The retrograde AAVs (pAAV-CAG-tdTomato and pAAV-CAG-EGFP) and the anterograde AAV (pENN.AAV.CB7.Cl.mCerulean.WPRE.RBG) were a gift from Drs. Edward Boyden, Massachusetts Institute of Technology (viral preps, catalog #59 462-AAVrg and #37825-AAVrg, Addgene), and James M. Wilson, University of Pennsylvania (viral prep, catalog #10 557-AAV1, Addgene), respectively. Fluoro-Gold and Fluoro-Ruby (Fluorochrome) were diluted in double distilled water to 4% and 10% concentrations, respectively.

Surgical and injection procedures. Animals were anesthetized with isoflurane (4–5% induction, 1–2% maintenance) and secured in a stereotaxic frame (David Kopf Instruments). The scalp was retracted to expose the skull, and small craniotomies were made above the target regions of the brain. Different cohorts of rats received different combinations of viral tracers in the dorsal and ventral subdivisions of the prefrontal cortex and hippocampus according to stereotaxic coordinates of Paxinos and Watson's (2005) rat brain atlas. All anteroposterior (AP) and medioateral (ML) readings were taken from bregma. All dorsoventral (DV) readings were taken from the dural surface. The injections were made using a 0.5 µl or 1 µl precision microsyringe (SGE Analytical Science).

Different groups of rats received two unilateral injections of reporter-specific trans-synaptic viruses (PRV and/or HSV-1) or monosynaptic tracers (FG and FR) into the left or right hemisphere or a combination of monosynaptic AAVs (AAVrg and AAV1). All relevant details concerning the injection sites including stereotaxic coordinates, tracer volume and virus titer can be found in Table 1. All tracers were infused over 3–5 min and allowed to diffuse for at least 5 min. The syringe was then carefully removed, and the scalp incision was closed with surgical staples. When rats were fully recovered, they were returned to their home cages. Following surgery, rats were given injections of carprofen (analgesic; 5 mg/kg, s.c.) and housed in a Biosafety Level 2 containment holding room.

Perfusion and histological procedures. After the appropriate survival period, rats were deeply anesthetized with a lethal overdose of sodium pentobarbital (VetOne) and perfused transcardially with 0.9% saline, followed by 4% paraformaldehyde in 0.01 M PBS. The brains were extracted, postfixed in 4% paraformaldehyde, and dehydrated in 30% sucrose in PBS at 4°C for ~2 d. Brains were frozen and stored at −80°C until cutting. Five series of 40-µm-thick sections were cut rostrocaudally in the coronal plane using a cryostat (Leica) and collected in wells containing 0.01 M PBS. One tissue series was mounted on gelatin-coated slides and coverslipped with VECTASHIELD HardSet Antifade Mounting Medium with DAPI (Vector Laboratories). Tissue sections were examined with a Zeiss Axio Imager Z.2 (Carl Zeiss MicroImaging) and photographed with a Zeiss AxioScan (10× magnification) with appropriate filters to detect the different fluorescent signals.

Quantification and illustration. We used Imaris software version 9.2.1 (Bitplane), which provided an unbiased sampling method for quantifying the density of neurons in each region of interest (ROI). We selected three to four sections for each ROI (septum, diagonal band of Broca, thalamus, amygdala, dorsal and ventral hippocampus) and quantified the entire ROI. We first used the surface tool of Imaris to delineate the ROI and overlaid sections from the Paxinos and Watson (2005) digital atlas onto our images. The spot tool was then used to identify green- and red-labeled neurons (spot diameter set at 10 µm or 15 µm) based on fluorescent signals above threshold. The intensity of the threshold was adjusted automatically for each batch of images to selectively identify dorsal and ventral PFC-projecting neurons. Finally, the Imaris colocalization tool was used to count the number of each cell type (red only, green only, and colocalized yellow) within the different ROIs. For each ROI, the proportion of each category of cells was obtained by dividing the number of neurons by the total cell count, then averaging for each animal for each survival time point. Similarly, cell density was obtained by dividing the number of neurons by the surface ROI. For those experiments involving AAV injections, one section was selected for each bregma level, and triple spots (i.e., three color channels) were calculated using an object–object statistics option with multiple filters for the shortest distance for each color. For illustration purposes, the green, red, and double-labeled neurons were transferred to selected atlas plates according to the automatic object detection feature in Stereo Investigator software (MBF Bioscience) and verified and corrected manually when necessary. The resulting traces were added to the corresponding atlas sections of Paxinos and Watson (2005) using Adobe Illustrator.

Results

To identify PFC circuit organization, we injected fluorescent recombinant PRVs, unilaterally, into the dPFC and vPFC, respectively, and examined the distribution of labeled neurons at different survival times (Fig. 1*A*). The selectivity of these viruses to label different populations of projecting neurons is highlighted in Figure 1*B*, which shows that cells infected with PRV expressing mRFP are distinct from those infected with PRV expressing GFP. The locations of the injection sites for each animal are schematically illustrated in Figure 1*C* with their corresponding survival time. The dPFC injections were localized in the cingulate cortex (Cg1), rostral and dorsal to the genu of the corpus callosum, and the most dorsal extent of the PrL. In one case (8434-1), the virus injection encroached the secondary motor cortex (M2). In the vPFC, the injections targeted the IL, encroaching slightly into the most ventral PrL and dorsal peduncular cortex (DP). The animals were killed at 24 h ($n = 3$), 48 h ($n = 5$), or 60 h ($n = 4$). At 24 h survival time, fluorescence at the infection site was only found in cells whose cell bodies were proximal to the injection site and did not transport beyond. In contrast, the distribution and density of fluorescently labeled neurons for those animals killed at 48 h and 60 h allowed us to determine the first- and second-order projection sites at these time points, respectively. Disynaptic transport was determined by observing infected cells in brain regions following the longer survival time of 60 h and comparing them with the distribution pattern at 48 h (Fig. 1*A*). In the following sections, we first report the restricted pattern of disynaptic labeling observed in the dHC followed by the pattern of monosynaptic labeling in potential relays that may link the dHC and PFC.

Dorsal hippocampus connects disynaptically to prefrontal neurons

We found, quite unexpectedly, that neurons in the dHC connect indirectly to both dorsal and ventral regions of the PFC. For the 60 h survival time, but not the 48 h survival time, we observed a large number of both red- and green-labeled infected neurons in the pyramidal layer of the dHC (Fig. 2*A*), thereby demonstrating that the dHC provides a second-order input to both dorsal and ventral regions of the PFC. Moreover, many cells in the dHC were colabeled with red and green, indicating a disynaptic retrograde convergence from the two prefrontal subregions onto the same hippocampal neurons. Of most interest was the pattern of cell labeling that was restricted to the CA2/CA3 area of the dHC (henceforth referred to as dCA3), which was preserved along its anterior–posterior axis. A representative example of this restricted pattern of expression can be seen in Figure 2*B*, which shows large numbers of red-, green-, and yellow-labeled neurons concentrated within the pyramidal dCA3 layer. In contrast, very few labeled cells were observed in the dCA1 region (Fig. 2*C*). We then extended these results with a cell count of the fluorescently labeled neurons in different subregions of the dHC, again confirming that the pattern of expression was localized to the dCA3 region (Fig. 2*D*). Of the total number of dHC neurons, a third (32.5%) of the retrogradely labeled neurons were green vPFC-

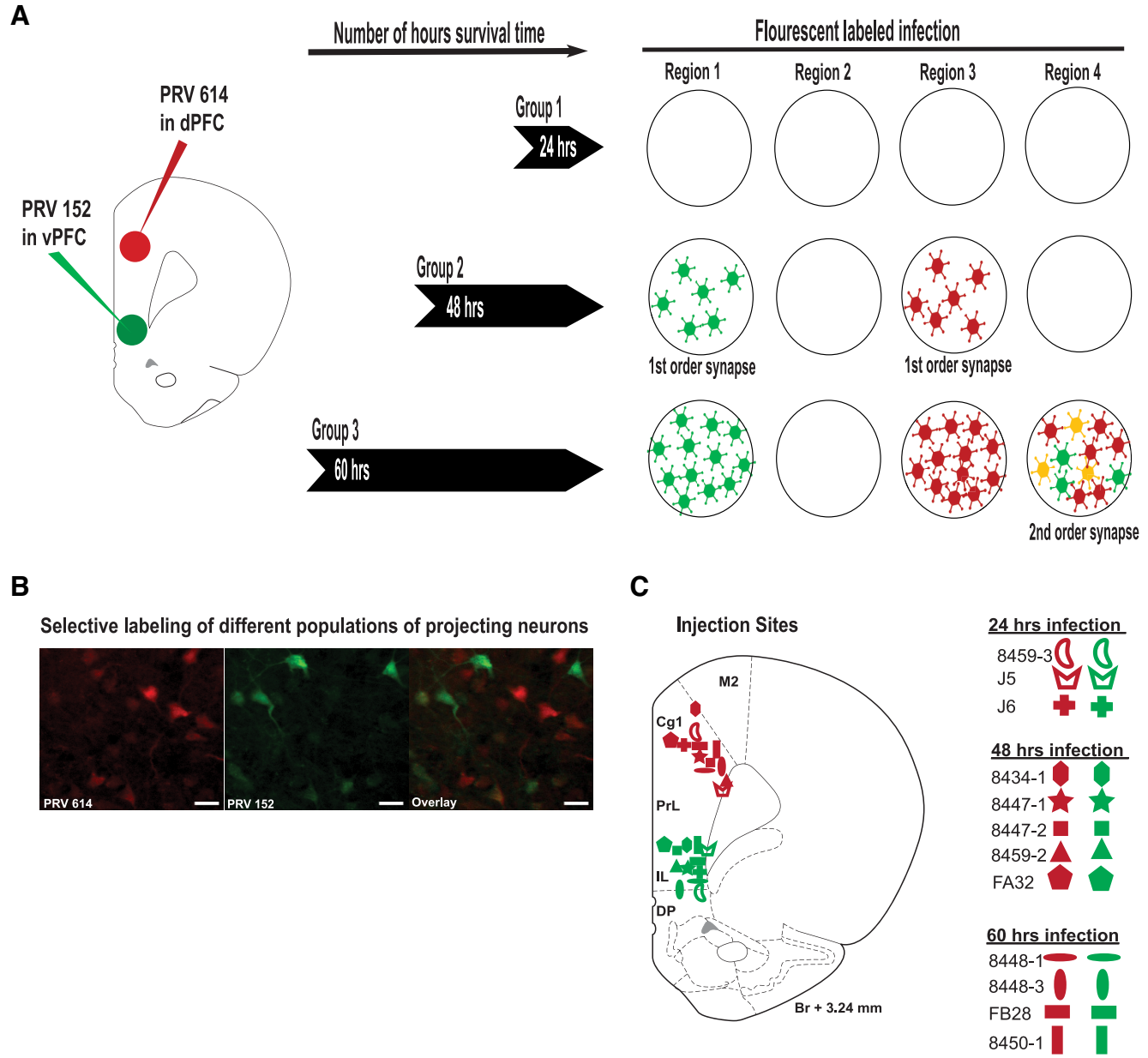

Figure 1. Cells infected with PRV expressing mRFP (red) are distinct from those infected with PRV expressing GFP (green). ***A***, Schematic illustrating design and logic of trans-synaptic viral method. After red and green PRVs were injected into dorsal and ventral PFC, respectively, brains were extracted following 24 h (Group 1), 48 h (Group 2) or 60 h (Group 3) to determine viral transport. A lack of fluorescently labeled infection indicates no viral replication and therefore no viral transport to that region (24 h). At 48 h, the expression of green- and red-fluorescent-labeled neurons in brain region 1 and region 3 indicates first-order connections to vPFC and dPFC, respectively. At 60 h, viral expression of red, green, and yellow cells in brain region 4 confirm second-order connections to both divisions of the PFC, whereas regions 1 and 3 increase density of first-order viral expression. Note that brain region 2 fails to show any fluorescent-labeled infection at any survival point and therefore does not connect to PFC. ***B***, Photomicrographs showing representative labeling of different populations of PRV-infected cells 48 h after injection. Left, Red cells are infected with PRV-614. Middle, Green cells are infected with PRV-152. Right, An overlay of PRV-614 and PRV-512 cells confirming the selectivity of the different projecting neurons. Scale bar, 20 μm. ***C***, Placement of injection sites for each animal in each group with survival times of 24, 48, and 60 h. Each animal that received unilateral injections of red- and green-expressing PRV in the dPFC and vPFC, respectively, is represented by an identical red and green symbol and its corresponding identification number.

projecting cells located in the dCA3, thus highlighting its important influence on the vPFC target.

Although this study focuses on disynaptic transport to the dCA3, we also observed disynaptic labeling in other brain areas. For example, a significant number of second-order GFP-expressing infected neurons were labeled in the dorsomedial hypothalamus and periventricular zone, neither of which project directly to the PFC (Saper, 1985; Shimogawa et al., 2015). Discrete GFP and mRFP second-order labeled neurons were also observed in the nucleus accumbens, primarily in the shell region (data not shown).

To our knowledge this is the first observation of indirect projections from the dCA3 to the rat prefrontal cortex. We next turn to how these cortical structures may be interlinked by examining the expression of first-order labeled neurons 48 h after PRV injection.

Potential relays between dorsal hippocampus and prefrontal cortex

Forty-eight hours after PRV injections into the dorsal and ventral PFC, we observed specific monosynaptic retrograde labeled neurons in the vHC and amygdala and in distinct nuclei within the

thalamus, lateral septum, and basal forebrain (Fig. 3). Several of these structures can be construed as potential relays linking the dCA3 with the PFC. In some cases, the labeling differed substantially between the dorsal and ventral PFC injections. In addition, the presence of double-labeled neurons indicated PFC convergence onto the same monosynaptically connected neuron. Below we describe the pattern of fluorescently labeled cells observed in the potential relay sites.

Ventral hippocampus

Along the rostrocaudal axis of the vHC, and consistent with previous studies, a significant number of GFP-expressing neurons were located in the CA1 pyramidal layer and ventral subiculum (Fig. 3*A–C*). Thus, as previously reported, we can confirm that the ventral CA1 (vCA1) and ventral subiculum project directly to the vPFC (Swanson, 1981; Jay and Witter, 1991; Cenquizca and Swanson, 2007). In the dorsal and intermediate level of the caudal CA1, fewer vPFC-projecting neurons could be observed, especially at the more caudal part, whereas GFP-expressing neurons were still prominent in the ventral subiculum. At this level of the hippocampus, there was also sparse labeling of red fluorescently labeled neurons that projected to the dPFC only, and a scattering of double-labeled neurons that projected simultaneously to both dorsal and ventral PFC (Fig. 3*C*). Importantly, 48 h postinoculation, all areas within the dorsal anterior hippocampus (−2.40 to −4.44 mm from bregma) were devoid of any infection (Fig. 2*A*).

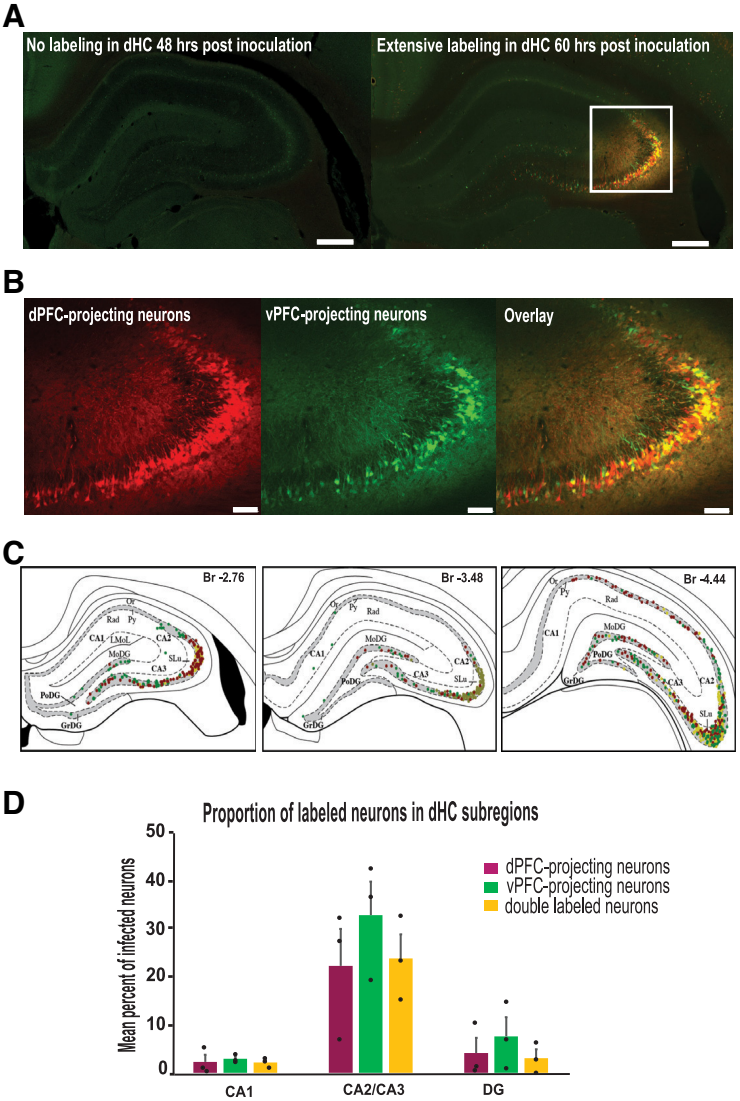

Figure 2. Dorsal hippocampus connects disynaptically to prefrontal neurons. ***A***, Representative photomicrograph showing lack of PRV-infected neurons in the dHC 48 h postinoculation (left) relative to the significant localization of PRV-infected neurons in the dCA3 field (right). Scale bar, 200 μm. ***B***, Magnified images of dPFC-projecting (expressing mRFP), vPFC-projecting (expressing GFP), and double-infected neurons in yellow (overlay) in dCA3. Scale bar, 100 μm. ***C***, Pattern of labeling along the rostral-caudal extent of the anterior part of dHC. Notice how the pattern of infection is localized to dCA3 and dentate gyrus. ***D***, Graph shows mean proportions of labeled neurons in various subfields of the dHC. Error bars represent standard error of the mean (SEM). Black dots represent data for each animal ($n = 3$). GrDG, granular layer of the dentate gyrus; LMoL, lacunosum moleculare layer of the hippocampus; MoDG, molecular layer of the dentate gyrus; Or, oriens layer of the hippocampus; PoDG; polymorph layer of the dentate gyrus; Py, pyramidal cell layer of the hippocampus; Rad, radiatum layer of the hippocampus; SLu, stratun lucidum of the hippocampus.

Lateral septum and nuclei of the diagonal band

In the lateral septum, retrogradely labeled neurons were found almost exclusively on the ipsilateral side of the PRV injection (Fig. 3*D*). Specifically, a small but significant number of vPFC-projecting neurons were expressed in the dorsal part of the lateral septum (Fig. 3*D*, *E*, top) as shown previously (Gaykema et al., 1990). In the same coronal plane but moving ventrally into the anterior basal forebrain (Fig. 3*D*,*E*, bottom), a moderate amount of labeling was observed in the vertical limb of the diagonal band and more caudally in the horizontal diagonal band. Again, the labeling was stronger in the ipsilateral side, and the labeled neurons were primarily vPFC-projection neurons. In contrast, very few dPFC-projecting neurons were found in the anterior basal forebrain including the medial septum (Bloem et al., 2014).

Amygdala

The observed monosynaptic distribution of retrogradely infected neurons in the amygdala was highly consistent with previous studies (Krettek and Price, 1977; McDonald, 1987, 1991; Reppucci and Petrovich, 2016). We observed a strong presence of red fluorescence dPFC-projecting neurons expressed primarily in the most rostral part of the basolateral amygdala (Fig. 3*G*,*H*, top). Very few if any red-labeled cells were observed caudally in this region especially after 3.00 mm from bregma. In contrast, green fluorescence vPFC-projecting neurons were distributed mostly in the basomedial and lateral nuclei of the amygdala at the rostral level (Fig. 3*H*, bottom). More caudally (in the intermediate and posterior amygdala), there was a large presence of vPFC-projecting neurons spread throughout both the dorsal and ventral parts. There was some scattering of double-labeled neurons in the lateral dorsal and basolateral nuclei (rostrally) and in the most ventral extent of the posterior portion of the basolateral nucleus. For the most part, nuclei within the basolateral and basomedial

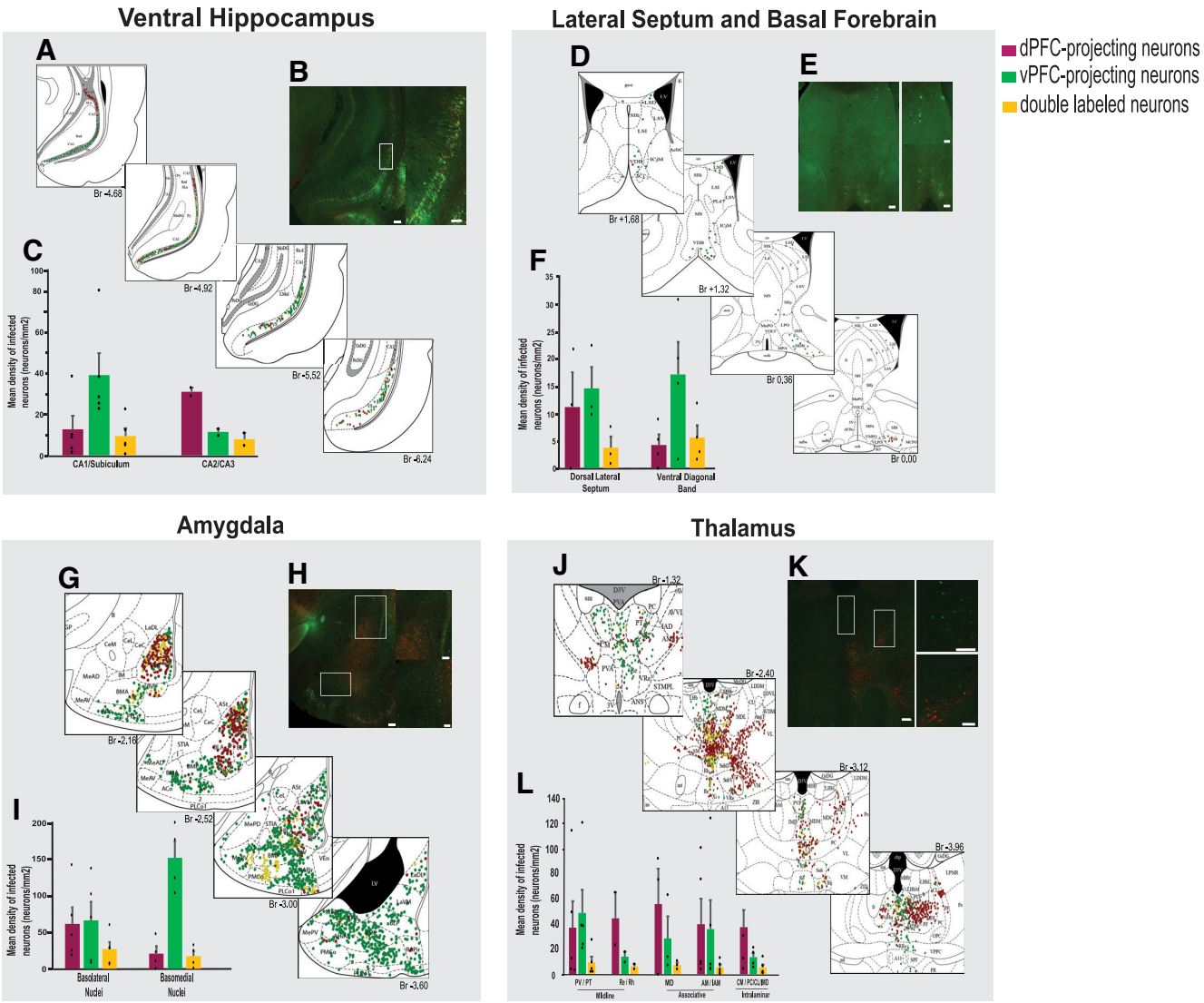

Figure 3. Potential relays between dorsal hippocampus and prefrontal cortex. ***A–L***, Pattern of monosynaptic retrograde labeled neurons, photomicrographic magnification, and mean density of infected neurons for ventral hippocampus (***A–C***), lateral septum and basal forebrain (***D–F***), amygdala (***G–I***), and thalamus (***J–L***). Graphs show mean densities of labeled neurons in the different subregions. Error bars represent SEM. Black dots represent data for each animal ($n = 2–4$). 3V, 3rd ventricle; A11, A11 dopamine cells; A1, A13 dopamine cells; aca, anterior commisure, anterior part; AcbC, accumbens, core; ACo, anterior cortical amygdaloid nucleus; AHiAL, amygdalohippocampal area, anterolateral part; AI, alar nucleus; AM,anteromedia; AM, anteromedial thalamic nucleus; AngT, angular thalamic nucleus; ANS, accessory neurosecretory nuclei; ASt, amygdalostriatl transition area; AV, anteroventral thalamic nucleus; AVDM, anteroventral thalamic nucleus, dorsomedial part; AVPe, anteroventral periventricular nucleus; AVVL, anteroventral thalamic nucleus, ventrolateral part; B, basal nucleus (Meynert); BLA, basolateral amygdaloid nucleus, anterior part; BLP, basolateral amygdaloid nucleus, posterior part; BLV, basolateral amygdaloid nucleus, ventral part; BMA, basomedial amygdaloid nucleus, anterior part; BMP, basomedia amygdaloid nulceus, posterior part; cc, corpus callosum; CeC, central amygdaloid nucleus, capsular part; CeL, central amygdaloid nucleus, lateral division; CeM, central amygdaloid nucleus, medial division; chp, choroid plexus; CL, centrolateral thalamic nucleus; CM, central medial thalamic nucleus; D3V, dorsal 3rd ventricle; E, ependyma and subependymal layer; f, fornix; fi, fimbria of the hippocampus; gcc, genu of the corpus callosum; GP, globus pallidus; HDB, nucleus of the horizontal limb of the diagonal band; IAD, interanteromedial thalamic nucleus; ICjM, islands of Calleja, major island; IM, intercalated amygdaloid nucleus, main part; IMD, intermediodorsal thalamic nucleus; LaDL, lateral amygdaloid nucleus, dorsolateral part; LaVL, lateral amygdaloid nucleus, ventrolateral part; LaVM, lateral amygdaloid nucleus, ventromedial part; LDDM, laterodorsal thalamic nucleus, dorsomedial part; LDVL, laterodorsal thalamic nucleus, ventrolateral; LHbL, lateral habenualr nucleusm lateral part; LHbM, lateral habenular nucleus, medial part; LPMR, lateral posterior thalamic nucleus, mediorostral part; LPo, lateral preoptic area; LSD, lateral septal nucleus, dorsal part; LSI, lateral septal nucleus, intermediate part; LSV, lateral septal nucleus, ventral part; LV, lateral ventricle; MCPO, magnocellular preoptic nucleus; MDL, mediodorsal thalamic nucleus, lateral part; MDM, mediodorsal thalamic nucleus, medial part; MeAD, medial amygdaloid nucleus, anterodorsal; MeAV, medial amygdaloid nucleus, anteroventral; MePD, medial amygdaloid nucleus, posterodorsal; MePV, medial aygdaloid nucleus, posteroventral; mfb, medial forebrain bundle; MHb, medial habenular nucleus; MnPO, median preoptic nucleus; MPA, medial preoptic area; MS, medial septal nucleus; mt, mammillothalamic tract; och, optic chiasm; OPC, oval paracentral thalamic nucleus; PC, paracentral thalamic nucleus; PF, parafascicular thalamic nucleus; PLCo, posterodorsal cortical amygdaloid nucleus; PMCo, posteromedial cortical amygdaloid nucleus; Po, posterior thalamic nuclear group; PoMn, posteromedian thalamic nucleus; PR, prerubral field; PT, paratenial thalamic nucleus; PV, paraventricular thalamic nucleus; PVA, paraventricular thalamic nucleus, anterior part; PVP, paraventricular nucleus, posterior part; RAPir, rostral amygdalopiriform area; Re, reuniens thalamic nucleus; Rh, rhomboid thalamic nucleus; RRe, retruniens area; SFi, septofimbrial nucleus; SHi, septohippocampal nucleus; SHy, septohypothalamic nucleus; SIB, substantia innominata, basal part; sm, stria medullaris of the thalamus; SO, supraoptic nucleus; SPF, subparafascicular thalamic nucleus; STIA, bed nucleus of the stria terminalis, intraamygdaloid division; VDB, nucleus of the vertical limb of the diagonal band; VEn, ventral endopiriform nucleus; VL, ventrolateral thalamic nucleus; VLPO, ventrolateral preoptic nucleus; VM, ventromedial thalamic nucleus; VOLT, vascular organ of the lamina terminalis; VPPC, ventral posterior nucleus of the thalamus, parvicellualr part; vRe, ventral reuniens thalamic nucleus; VS, ventral subiculum; Xi, xiphoid thalamic nucelus; ZID, zona incerta, dorsal part; ZIR, zona incerta, rostral part.

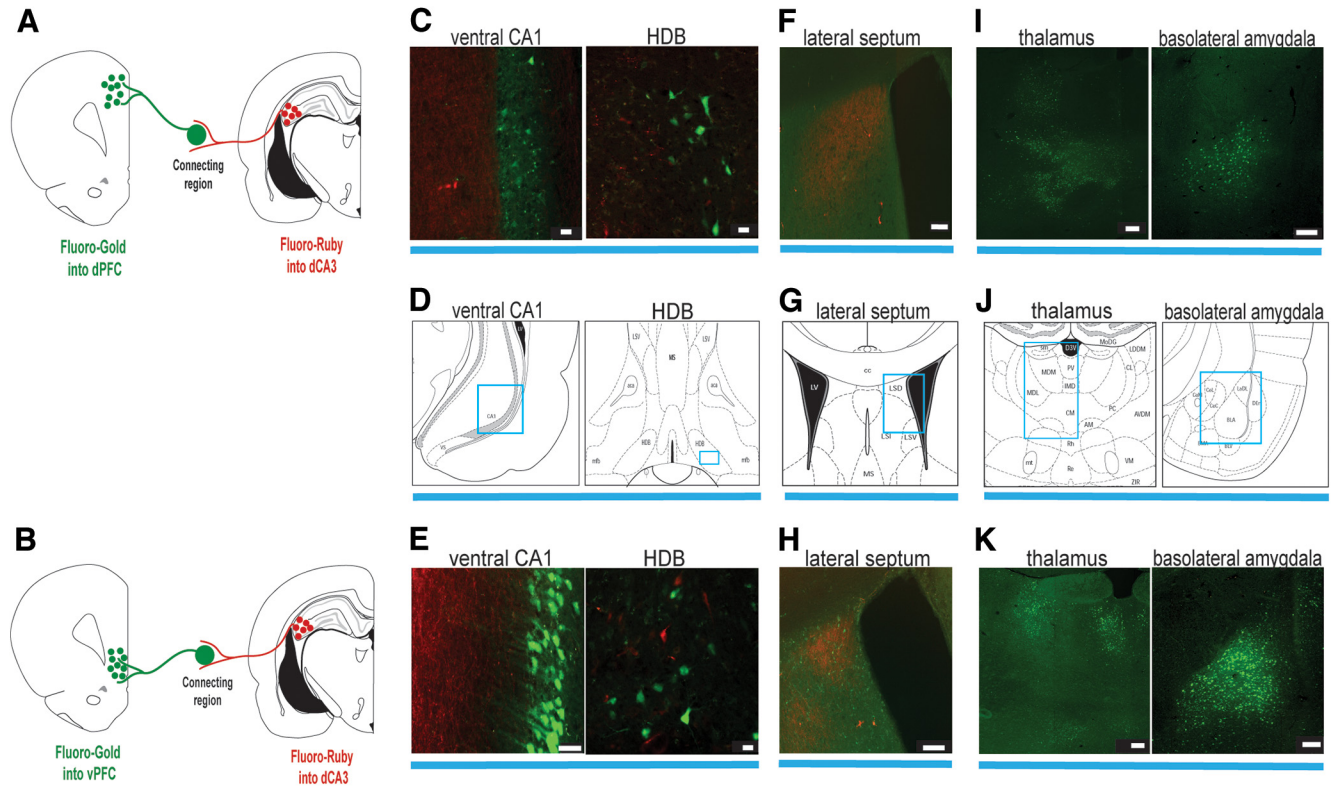

Figure 4. First-order connections to the PFC were confirmed with injections of the retrograde tracer FG and combined with anterograde tracer FR to establish putative connecting relays. ***A***, ***B***, Tracing strategy showing FG injected in the dorsal and ventral PFC and FR injected in the dorsal CA3 region of the hippocampus. ***C***, ***E***, High-magnification photomicrographs showing dCA3 fibers/terminals (red) in the vicinity of neurons retrogradely labeled from the dorsal and ventral PFC (green) in the ventral CA1 (left) and HDB (right). Scale bars: ***C***, 20 and 50 μm; ***E***, 20 μm. ***F***, The lateral septum shows FR anterogradely labeled fibers/terminals from the dCA3 only but not retrogradely labeled neurons projecting to the dPFC. Scale bar, 100 μm. ***H***, Lateral septum shows dCA3 fibers/terminals (red) in close proximity to neurons retrogradely labeled projecting to ventral PFC (green). Scale bar, 100 μm. ***I***, ***K***, The thalamus and basolateral amygdala show FG retrogradely labeled neurons projecting to the PFC only but not FR anterogradely labeled fibers/terminals from dCA3. Scale bars: 200 μm. ***D***, ***G***, ***J***, Representative atlas plates highlighting magnified region in blue square or rectangle. AM, anteromedial thalamic nculeus; DEn, dorsal endopiriform nucleus.

amygdala complex project selectively to dorsal and ventral prefrontal regions, respectively (Fig. 3*I*). Labeled neurons were not observed in the central amygdala (Amaral and Insausti, 1992).

Thalamus

As expected, monosynaptic labeling following PFC injections was extensive along the rostrocaudal extent of the thalamus, mainly ipsilateral to the side of the injection. Most of the labeled neurons expressed mRFP thereby projecting directly to the dPFC. One major observation was the density of retrogradely labeled dPFC-projecting neurons located in the lateral part of the mediodorsal nucleus (Fig. 3*J*). A large number of dPFC-projecting neurons were also present in the intralaminar thalamic nuclei, namely, the centromedial and paracentral nuclei, as well as the intermediodorsal thalamus and reuniens/rhomboid located along the midline. In contrast, the paraventricular and paratenial nuclei of the midline thalamus contained both red and green fluorescently labeled neurons and a small portion of double-labeled neurons indicating that this midline thalamic structure projects diffusely to both dorsal and ventral PFC. These findings are in keeping with previous reports of thalamic projections to the PFC (Shibata, 1993; Vertes et al., 2015; Alcaraz et al., 2016; Kuramoto et al., 2017).

The labeling patterns for regions described above were confirmed as first order connections to the PFC using FG as a conventional retrograde tracer. When combined with dCA3 injections of the anterograde tracer FR, we were able to discern putative connecting relays by observing the close proximity of FR-labeled terminals and fibers from the dCA3 (labeled red) and FG-labeled cell bodies projecting to the PFC (labeled green; Fig. 4*A*,*B*). The most pronounced putative relay, and consistent with labeling pattens following PRV injections, was the ventral CA1, which showed extensive convergence of dCA3 fibers/terminals and retrogradely labeled neurons to both divisions of the PFC (Fig. 4*C*–*E*). The horizontal diagonal band (HDB) could also be considered a potential relay, but here the labeling was less intense with fibers/terminals and neurons loosely distributed within the basal forebrain area. Intriguingly, fibers/terminals from dCA3 in the lateral septum were located in the vicinity of ventral PFC-projecting neurons only (Fig. 4*F*–*H*). Finally, monosynaptic FG-labeled PFC-projecting neurons were observed in the thalamus and basolateral amygdala (Fig. 4*I*–*K*), but in both cases, there was an absence of fibers and terminals from the dCA3, suggesting that they do not receive input from the dCA3 region of the hippocampus and therefore are not relaying its information to the PFC. Together, the evidence suggests three putative relays—vCA1, basal forebrain, and lateral septum.

Connecting neurons in rostrocaudal vHC differentiate dorsoventral PFC

Injecting recombinant fluorescent PRVs revealed multiple relays within deep structures of the limbic system that could putatively enable the transmission of signals from the CA3 region of the dHC to the PFC but cannot provide with certainty the specific connecting link. Therefore, to determine the specific neurons connecting these regions, we combined dCA3 injections of anterograde HSV-1 and PFC injections of retrograde PRV and

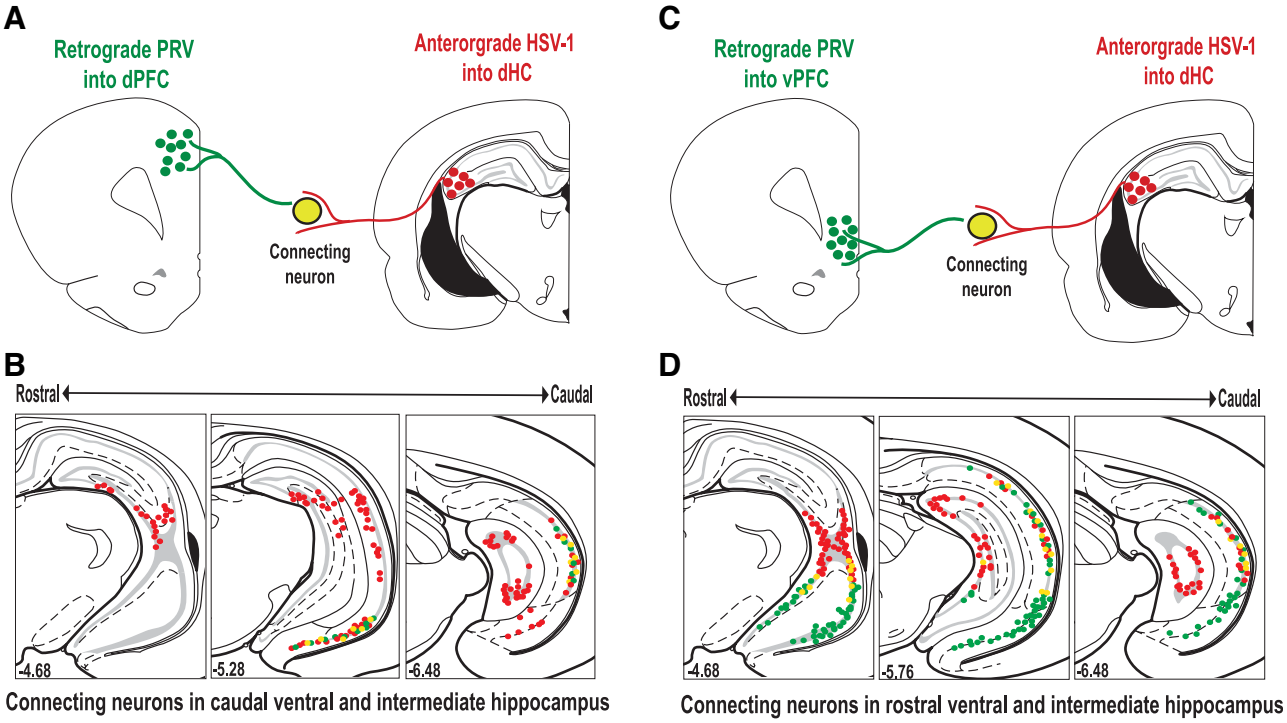

Figure 5. Second-order dorsal hippocampal projections to prefrontal cortex determined by HSV and PRV tracers. ***A***, ***C***, Tracing strategy. ***B***, ***D***, Distribution of PRV (red), HSV (green), and double-labeled (yellow) neurons in ventral and intermediate hippocampus. Double-labeled neurons connecting the dCA3 and dPFC were distributed caudally in the ventral and intermediate CA1 of the hippocampus, whereas those connecting dCA3 with vPFC were found more rostrally in the same regions.

identified double-labeled neurons in those brain regions that served as the connecting link between the two regions (Fig. 5).

When the injections were made in dPFC and dCA3 (Fig. 5*A*), double-labeled neurons were observed primarily in the pyramidal layers of the CA1 region of the hippocampus (Fig. 5*B*). These cells, specifically connecting the dCA3 and dPFC, were present in the vCA1 rostrally, but were mostly distributed along the caudal extent of ventral and intermediate CA1. A similar pattern was observed when the injections were made in the vPFC and dCA3 (Fig. 5*C*), but this time with stronger density and extension along the most rostral extent of the ventral and intermediate CA1 (Fig. 5*D*). Here, double-labeled neurons were intermingled with PRV and HSV single-labeled neurons. Few double-labeled neurons were also present in the ventral CA3 area. More caudally, there was a scattering of double-labeled neurons in vCA1 (Fig. 5*D*). Thus, there may exist separate connecting neurons linking the dorsal CA3 with dorsal and ventral PFC segregated rostrocaudally in the ventral and intermediate hippocampus.

Another putative connecting link that emerged from the combined dCA3 and PFC injections was the basal forebrain. In those cases, with combined dPFC and dCA3 injections, there was a scattering of PRV-labeled neurons located in close proximity to HSV-labeled neurons and fibers, specifically in the horizontal diagonal band of Broca (data not shown). Similarly, a few PRV-labeled neurons and HSV-labeled neurons and fibers were found in the vicinity of each other in the basal forebrain following dPFC and dCA3 injections. In these cases, labeled cells were observed rostrally in the ventral diagonal band and caudally in the HDB of Broca. However, double-labeled neurons, which indicate convergence of the two brain regions, were not observed, suggesting that although the primary connecting relay between the dCA3 of the hippocampus and PFC is the vCA1, the band of Broca and basal forebrain may be a minor link. We were also unable to detect double-labeled connecting neurons in the septum. These negative findings might be related to poor viral uptake within the PFC and dCA3 because viral concentration and density of innervation can influence the onset of viral replication (Card et al., 1998). This prompted us to use a combination of retrograde and anterograde AAVs to verify that the septum could be a possible connecting area between dCA3 and PFC.

Connecting relays in ventral CA1 and dorsal lateral septum

The combination of trans-synaptic PRV and HSV highlighted the significance of the vHC as a critical relay in the dCA3 to PFC pathway. Unfortunately, in our cases, the combination of these two trans-synaptic viruses, although useful to observe connecting neurons, resulted in weak expression. Therefore, to confirm and potentially expand the findings described above, we combined a retrograde AAV in the dPFC (tdTomato) and vPFC (EGFP) with an anterograde AAV (with trans-synaptic properties) in the dCA3 (cerulean; Fig. 6*A*). We looked for the presence of retrogradely labeled red, green, or colabeled neurons in the vicinity of anterogradely labeled cerulean fibers to confirm the connecting relays between the dCA3 and the PFC.

In the ventral and intermediate CA1, we observed a strong presence of vPFC-projecting cells (labeled green) and some dPFC-projecting cells (labeled red) in close proximity to dCA3 fibers and terminals (labeled blue; Fig. 6*B*). When the AAV-cerulean expression was stronger, we were able to identify cerulean-labeled neurons in the CA1 layers in addition to the expected cerulean fibers. The AAV1 serotype is known to transport trans-synaptically (Zingg et al., 2017). Consequently, we also observed neurons that were colabeled with both cerulean and GFP (cyan-labeled neurons), with both cerulean and tdTomato (magenta-labeled neurons), and with all the three fluorophores at once (Fig. 6*Ba,b*). If the labeling of those neurons truly results from anterograde trans-synaptic transport, they could represent neurons directly connecting dCA3 to vPFC, dCA3 to dPFC, and finally

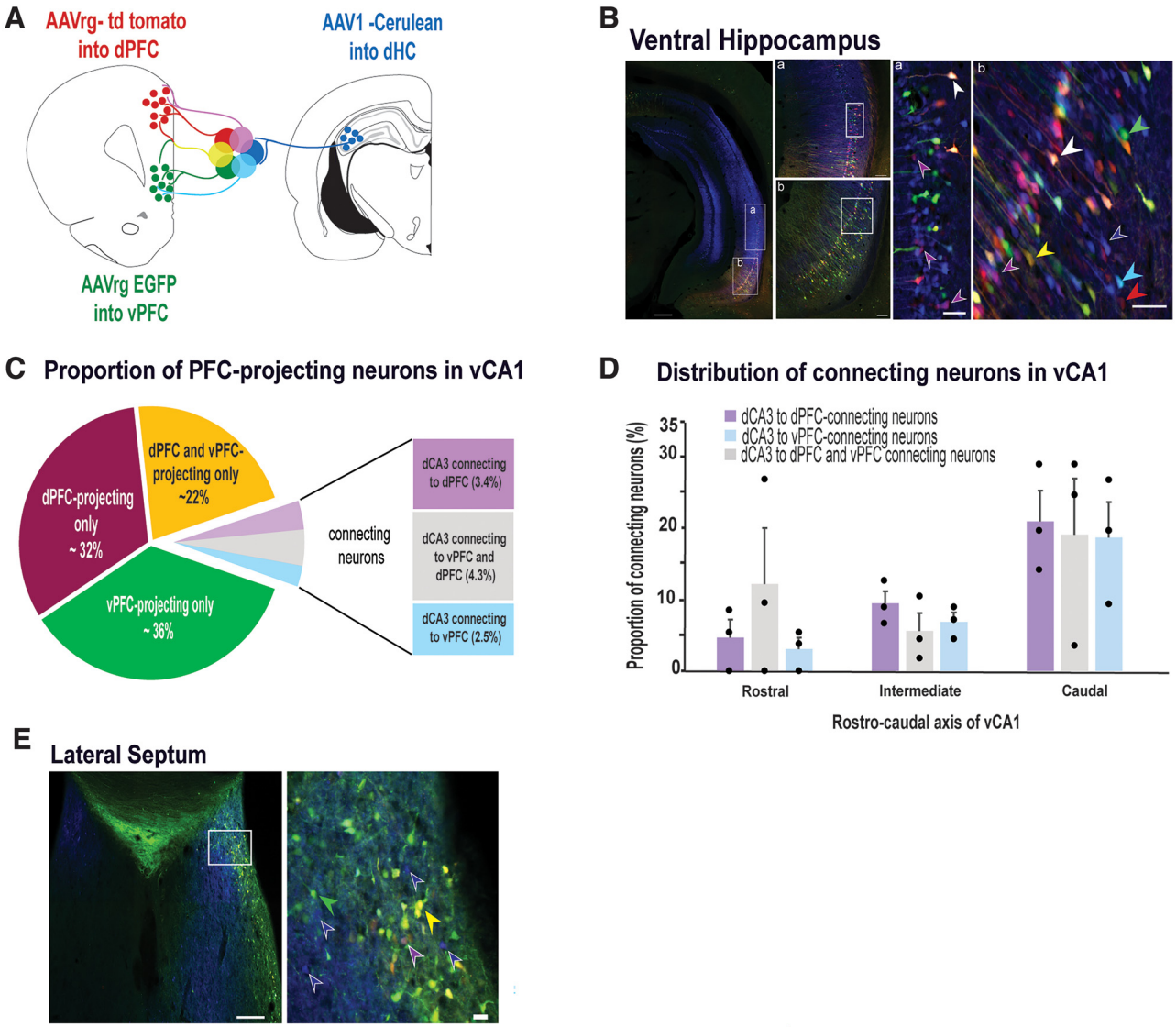

Figure 6. Connecting relays of the second order dCA3 projections to PFC determined by AAV injections. ***A***, Tracing strategy shows possible combinations of fluorescently labeled neurons following retrograde AAVs (AAVrg) injections into the dorsal and ventral PFC and trans-synaptic AAV1 injections into dCA3. ***B***, Photomicrographic magnifications of ventral and intermediate hippocampus. ***Ba***, Distribution of cerulean-labeled neurons and fibers in the intermediate CA1 layer. Labeled neurons are mostly retrogradely labeled vPFC-projecting cells (green) with some scattering of dPFC-projecting cells (red). There is also a scattering of dPFC-projecting double-labeled cells (magenta) indicated by arrowheads. ***Bb***, Distribution of double-labeled neurons (cyan and magenta) and anterogradely labeled fibers and terminals (blue) in the vicinity of retrogradely single-labeled (red and green) and double-labeled (yellow) neurons in the ventral CA1. Scale bars: 500 and 50 μm. Color-coded arrowheads indicate presence of neurons connecting dCA3 to dorsal PFC, ventral PFC, or both (magenta, cyan, and white, respectively), and putative anterogradely labeled neurons (blue), as well as retrogradely labeled neurons (red, green, and yellow). ***C***, Different categories among total number of PFC-projecting neurons identified in the vCA1. Those categories include PFC-projecting only neurons (green-, red-, and yellow-labeled neurons) as well as connecting neurons between dCA3 and PFC (magenta-, cyan-, and white-labeled neurons). ***D***, Proportion of putative connecting neurons (magenta, cyan, and white; error bars represent SEM. Black dots represent data for each animal ($n = 3$)) distributed along the rostrocaudal axis of the vCA1 (rostral, −4.68 to −5.28 mm; intermediate, −5.76 mm; caudal, −6.24 to −6.72 from bregma according to Paxinos and Watson, 2005). ***E***, Photomicrographic magnifications of the lateral septum showing retrogradely labeled green (indicated by the green arrowhead) and some colabeled neurons (yellow, indicated by the yellow arrowhead) and a single magenta-labeled neuron (magenta, indicated by magenta arrowhead) in the presence of extensive anterogradely labeled cerulean neurons and fibers (blue arrowheads) in the dorsal lateral portion of the septum. Scale bars: 200 and 20 μm.

dCA3 to both subdivisions to the PFC at once. A cell count revealed that among all the PFC-projecting cells identified in vCA1, ~10% of them connect dCA3 to PFC (Fig. 6*C*). Those putative connecting neurons were distributed into three categories, (1) those connecting dCA3 to dPFC (magenta-labeled neurons, 3.4%), (2) those connecting dCA3 to vPFC (cyan-labeled neurons, 2.5%), and (3) those connecting dCA3 to both dPFC and vPFC (white labeled, 4.3%). Moreover, we discovered that the connecting neurons were distributed along the rostrocaudal extent of vCA1, preferentially located in the caudal sector in our experimental cases (Fig. 6*D*). These data, similar to the PRV-HSV tracing data, suggest the existence of different pathways from dCA3 to different prefrontal divisions through a link in the vCA1.

Retrogradely labeled cells in the presence of anterogradely labeled fibers were also observed in the dorsal lateral septum (Fig. 6*E*). These neurons were mostly labeled with GFP, thereby suggesting a preferential projection to the vPFC. We counted the neurons in one brain that had sufficient expression of all three viruses within the septum, although the injection into the dPFC encroached substantially into the PrL, which could explain the strong presence of red-labeled cells. Of the PFC-projecting cells, 7% were labeled with cerulean injected in the dCA3 in this one

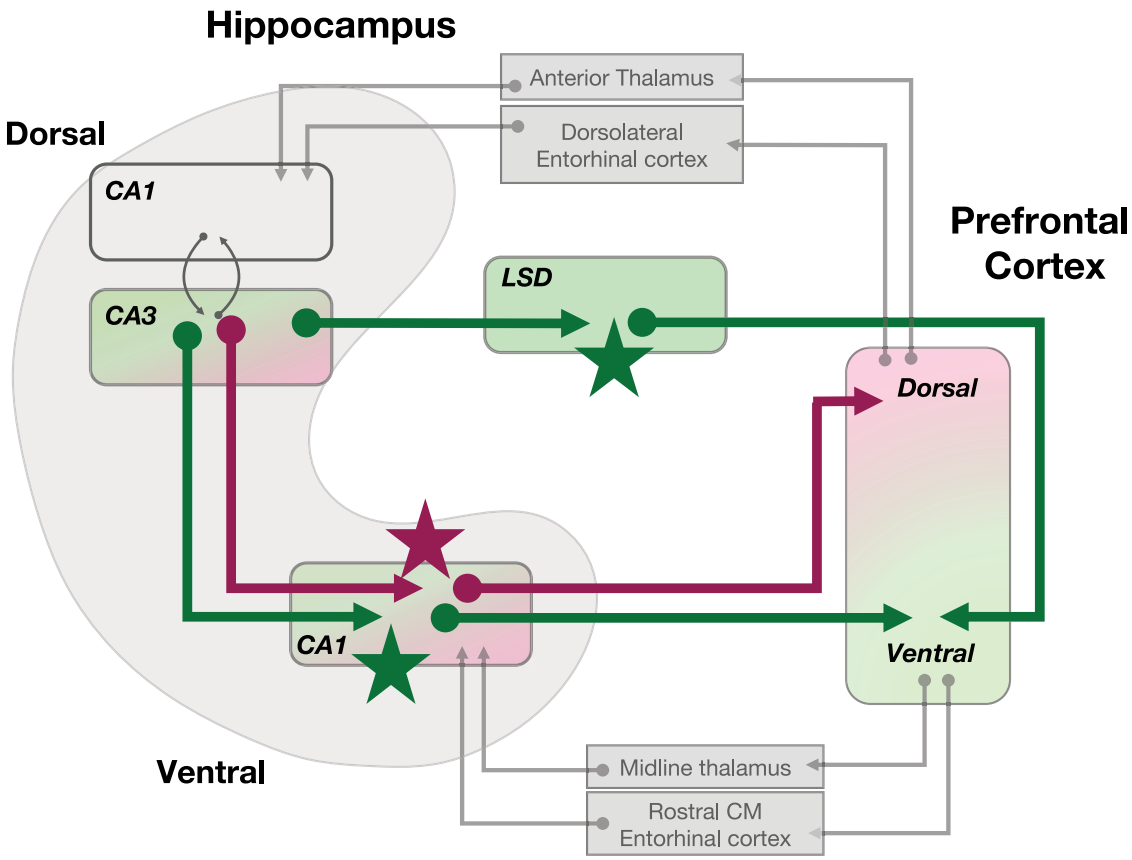

Figure 7. Illustration of parallel prefrontal pathways (bold green and red arrows) from the dorsal CA3 region of the hippocampus as shown in this study. The dCA3 connects disynaptically to the dorsal and ventral PFC via relays in the ventral CA1 or the dorsal lateral septum (LSD). Indirect input from dorsal and ventral PFC to the dorsal and ventral CA1 through relays in the thalamus and entorhinal cortex has been shown previously (Prasad and Chudasama, 2013). Bold stars highlight relays. CA1 to CA3 feedback projections from Lin et al. (2021).

animal only. This septal subdivision has been shown previously to receive strong projections from dorsal dCA3 (Ino et al., 1987; Risold and Swanson, 1997). Previous studies have also demonstrated light projections from dorsal lateral septum to PFC (Staiger and Nürnberger, 1991; Hoover and Vertes, 2007). Together with the FG-FR tracing study, these data strengthen the hypothesis that the dorsal lateral septum is a putative relay linking dCA3 to PFC.

Interestingly, in the diagonal band of Broca, we did not find retrogradely labeled cells in the presence of anterogradely labeled fibers in our different cases. Here, we observed blue-labeled fibers and neurons but very few if any green- or red-labeled neurons. This observation was rather surprising given the well-reported connections between this region and the PFC. This could be because of the location of the injection site in the PFC or maybe the transport of the retrograde AAV. We also note that because the dCA3 and septum have known reciprocal connections (Amaral and Witter, 1989; Risold and Swanson, 1997), the few cerulean-labeled neurons detected in the dorsolateral septum following injection of the AAV1 virus in the dCA3 might have been retrogradely labeled, which can occur under certain conditions with viruses of the AAV1 serotype (Zingg et al., 2017, 2020). This is also true for the recent discovery that vCA1 projects back to CA3 along the hippocampal transverse axis (Lin et al., 2021). Notwithstanding this important caveat, the presence of colabeled neurons (i.e., cyan and magenta), together with the cases involving injections of PRV and HSV, does not detract from the main finding that dCA3 targets both prefrontal divisions through relays in the vCA1 and dorsal lateral septum.

Discussion

Our findings demonstrate parallel multisynaptic pathways through which the dorsal hippocampus can influence activity in the prefrontal cortex, whose role in cognitive-executive behaviors is well established (Fig. 7). Both dorsal and ventral divisions of the prefrontal cortex receive disynaptic input from the CA3 region of the dorsal hippocampus. Systematic investigation revealed that the CA1 of the ventral hippocampus and dorsolateral septum were viable anatomical relays. Although the vPFC received disynaptic projections from the dorsal hippocampus through both of these relays, the dPFC only received input through the ventral hippocampal relay. Interestingly, the double labeling of cells further revealed that a substantial fraction of individual dorsal hippocampal neurons sent disynaptic projections to both dPFC and vPFC. This parallel organization of dorsal and ventral prefrontal pathways provides a new framework for understanding long-range influences over prefrontal interactions, including the specific contribution of the dorsal hippocampal CA3 region to prefrontal function. The findings reinforce and extend our growing perspective that temporal lobe structures can contribute extensively to the expression of prefrontal-executive function.

Parallel organization of the dorsal and ventral prefrontal pathways

We demonstrated that two parallel relay pathways, including one passing through the CA1 region of the ventral hippocampus and one in the dorsal lateral septum, are situated to carry dorsal hippocampal signals to the prefrontal cortex. The vCA1 relay was strong and highly robust, showing labeling across experiments

and tracers injected into both prefrontal subdivisions. Moreover, the combined multisynaptic tracer experiments using HSV (anterograde) and PRV (retrograde) revealed that many neurons were labeled anterogradely from a dCA3 injection and also retrogradely from PFC injections. This double labeling is good evidence for a synaptic relay pathway. Interestingly, the combined AAV experiments revealed that the vCA1 relay neurons projecting to dorsal and ventral PFC subdivisions constituted distinct populations, although the upstream (disynaptic) neurons in dCA3 were often double labeled.

It is well established that field CA1 is a major output of CA3 neurons. This projection is most often considered within the same transverse hippocampal section (Fanselow and Dong, 2010). However, the projection from CA3 to CA1 is not restricted to a transverse section, with the longitudinal component along the hippocampal axis differing with the proximodistal location of CA3 projection neurons. In fact, this anatomical organization has been surmised to facilitate the propagation of information along the transverse axis (Amaral and Witter, 1989; Ishizuka et al., 1990; Li et al., 1994; Wittner et al., 2007; Ropireddy et al., 2011).

While strong direct projections from vCA1 to cortical areas including the vPFC have been clearly established in rats (Hoover and Vertes, 2007) and similarly reported in monkeys (Barbas and De Olmos, 1990; Ghashghaei et al., 2007; Aggleton et al., 2015), the direct inputs from the dHC to prefrontal cortical areas has previously been reported as weak or nonexistent (Jay and Witter, 1991; Cenquizca and Swanson, 2007). However, recent studies have suggested otherwise (Barker et al., 2017; Ye et al., 2017; Bienkowski et al., 2018; Beerens et al., 2021) showing a direct dorsal CA1 projection to the PFC, and this might be relevant when considering signal processing in the PFC.

The retrograde labeling of vCA1 neurons was a robust and consistent finding in our study. Here, this labeling was observed with dorsal, as well as ventral, retrograde prefrontal injections, using PRV, retrograde AAV, and conventional tracers. The direct ventral hippocampal–prefrontal projection is not reciprocated, and the PFC has the capacity to influence activity in vCA1 through relay pathways, such as midline thalamic nuclei and the entorhinal cortex (Witter and Groenewegen, 1984; Wouterlood et al., 1990; Prasad et al., 2013; Prasad and Chudasama, 2013). Contrary to these data obtained in rats, a discrete monosynaptic projection from the PFC to dorsal CA1 in mice was recently reported by Malik et al. (2022). Whether this represents a species difference, and whether this projection exists in primates, is yet to be determined. Nonetheless, it is interesting to contemplate the idea of several direct and indirect pathways between the PFC and hippocampus each processing different or overlapping information. Together, these projections suggest the possibility that recurrent anatomical pathways can play an important role in cortico-hippocampal function.

We also identified a viable relay from the dCA3 to vPFC through the dorsal lateral septum. In general, the labeling patterns suggested that this pathway was weaker than the vCA1 relay but was clearly present in the combined PRV and retrograde AAV injections. The absence of double-labeled connecting neurons using the combined HSV and PRV injections is a puzzle and may be because of viral tropisms or other factors such as superinfection inhibition that limit reporter expression in certain cell types (Li et al., 2019; Ryu et al., 2017). Tracing studies have shown that the projection of the hippocampus on the lateral septum shows a high degree of topographic organization such that different regions of the hippocampus project in an ordered manner to different zones within the lateral septal nucleus (Swanson and Cowan, 1977). Our finding of a dCA3 projection to the dorsal lateral septum is consistent with this topography. Notably, this topography was not preserved in the projections to the prefrontal cortex. The dense innervation of the lateral septum by the vPFC has been shown to modulate fear and anxiety-like behaviors (Chen et al., 2021). The restricted projection of the dorsal lateral septum back to the vPFC may also participate in the regulation of those behaviors and might even have an impact on prefrontal-cognitive behaviors, a hypothesis that needs to be tested directly.

The influence of spatial and temporal context on prefrontal function

The prominent disynaptic pathway to the PFC originating in the dorsal hippocampus has theoretical implications for how the PFC may incorporate contextual information into its cognitive-executive behaviors. The dHC is best known for its role in navigation and memory processes, respectively placing events and experiences within a spatial and temporal context. The dorsal CA3 field is involved in the rapid encoding of novel environmental information, associations, and pattern separation (Hunsaker et al., 2008; Nakamura et al., 2013; Marrone et al., 2014; Lee et al., 2015; Lu et al., 2015). Although these computations are central to many aspects of executive function, it has never been clear how information that is explicitly encoded in dCA3 cells can influence high-order cognitive behaviors associated with the PFC. Moreover, since dCA3 is also influenced by other structures including the amygdala (Petrovich et al., 2001; Pitkänen et al., 2000) and entorhinal cortex (Amaral and Witter, 1989; Kajiwara et al., 2008), which target different layers along the longitudinal axis of the hippocampus (Aggleton, 1986; Jones, 1993; Witter, 1993; Wang and Barbas, 2018) thereby influencing internal processing in the hippocampus, the convergence of highly processed spatial, contextual/episodic, and emotional information from these regions broadly add to the complex signal processing in the PFC.

The demonstration here of parallel prefrontal pathways from the dorsal hippocampus may help explain how such information is incorporated into a range of cognitive behaviors. Spatial context and memory bear on virtually every aspect of natural behavior that governs foraging, social interplay, and predator–prey interactions (Wang et al., 2013; Montagrin et al., 2018; Harland et al., 2021). Thus, the best studied features of the dorsal hippocampus are readily incorporated on aspects of behavior whose elements are believed to be mediated by the prefrontal cortex. The pathways identified in the present study may serve to inform and update prefrontal areas about the environmental and temporal context that are important for decision-making and other aspects of executive function. Many cognitive tasks that involve the PFC require the awareness of spatial variables including one's own current position within an environment, the recognition of novelty/familiarity, and context discrimination. Accordingly, cognitive-executive processes that enable behaviors such as decision-making, planning and organization, and flexibility depend on some representation of contextual space in the PFC (Jones and Wilson, 2005; Sauer et al., 2022).

Although space and time are the best studied variables represented in the dorsal hippocampus, it is also possible that the mapping of dCA3 inputs onto different prefrontal regions entails a higher level of abstraction that involves different types of spaces, such as social structures, mnemonic hierarchies, categorical principles, or planning sequences. In other words, the dCA3 input to the PFC may support

abstract observations that go beyond normal considerations of space and time. Previous work has explored such abstraction in relation to the cognitive maps present in the medial temporal lobe (Behrens et al., 2018; Avigan et al., 2020), suggesting that the computations underlying spatial memory may well extend to other domains of flexible behavior.

The functional interaction between dorsal hippocampus and the prefrontal cortex has not been explored in great detail. However, reports indicate that impairments in hippocampal-related processing of spatial information can serve as a predictor for the development of cognitive impairments seen in dementia, schizophrenia, and post-traumatic stress disorder (Dowson et al., 2004; Tamminga et al., 2010; Kheirbek et al., 2012; Das et al., 2014). Our findings of prominent disynaptic pathways to the prefrontal cortex may be an important clue for understanding how spatial information influences executive function during development. Future experiments will refine our understanding of these pathways, including their anatomical organizing principles, including systematically studying the layout of projections along the transverse axis of dCA3 and the laminar specificity relay-recipient neurons within the PFC. These and similar experiments would help to answer questions concerning the functional architecture of the distinct pathways to PFC, the nature of the information relayed, and the cognitive-emotional functions affected.

References

Aggleton JP (1986) A description of the amygdalo-hippocampal interconnections in the macaque monkey. Exp Brain Res 64:515–526.

Aggleton JP, Wright NF, Rosene DL, Saunders RC (2015) Complementary patterns of direct amygdala and hippocampal projections to the macaque prefrontal cortex. Cereb Cortex 25:4351–4373.

Alcaraz F, Marchand AR, Courtand G, Coutureau E, Wolff M (2016) Parallel inputs from the mediodorsal thalamus to the prefrontal cortex in the rat. Eur J Neurosci 44:1972–1986.

Amaral DG, Witter MP (1989) The three-dimensional organization of the hippocampal formation: a review of anatomical data. Neuroscience 31:571–591.

Amaral DG, Insausti R (1992) Retrograde transport of D-[3H]-aspartate injected into the monkey amygdaloid complex. Exp Brain Res 88:375–388.

Avigan PD, Cammack K, Shapiro ML (2020) Flexible spatial learning requires both the dorsal and ventral hippocampus and their functional interactions with the prefrontal cortex. Hippocampus 30:733–744.

Barbas H, De Olmos J (1990) Projections from the amygdala to basoventral and mediodorsal prefrontal regions in the rhesus monkey. J Comp Neurol 300:549–571.

Barbas H, Blatt GJ (1995) Topographically specific hippocampal projections target functionally distinct prefrontal areas in the rhesus monkey. Hippocampus 5:511–533.

Barker GR, Banks PJ, Scott H, Ralph GS, Mitrophanous KA, Wong LF, Bashir ZI, Uney JB, Warburton EC (2017) Separate elements of episodic memory subserved by distinct hippocampal-prefrontal connections. Nat Neurosci 20:242–250.

Barnett EM, Evans GD, Sun N, Perlman S, Cassell MD (1995) Anterograde tracing of trigeminal afferent pathways from the murine tooth pulp to cortex using herpes simplex virus type 1. J Neurosci 15:2972–2984.

Bedwell SA, Tinsley CJ (2018) Mapping of fine-scale rat prefrontal cortex connections: evidence for detailed ordering of inputs and outputs connecting the temporal cortex and sensory-motor regions. Eur J Neurosci 48:1944–1963.

Bedwell SA, Billett EE, Crofts JJ, Tinsley CJ (2014) The topology of connections between rat prefrontal, motor and sensory cortices. Front Syst Neurosci 8:177.

Beerens S, Vroman R, Webster JF, Wozny C (2021) Probing subicular inputs to the medial prefrontal cortex. iScience 24:102856.

Behrens TEJ, Muller TH, Whittington JCR, Mark S, Baram AB, Stachenfeld KL, Kurth-Nelson Z (2018) What is a cognitive map? organizing knowledge for flexible behavior. Neuron 100:490–509.

Berendse HW, Groenewegen HJ (1991) Restricted cortical termination fields of the midline and intralaminar thalamic nuclei in the rat. Neuroscience 42:73–102.

Bienkowski MS, Bowman I, Song MY, Gou L, Ard T, Cotter K, Zhu M, Benavidez NL, Yamashita S, Abu-Jaber J, Azam S, Lo D, Foster NN, Hintiryan H, Dong HW (2018) Integration of gene expression and brain-wide connectivity reveals the multiscale organization of mouse hippocampal networks. Nat Neurosci 21:1628–1643.

Bloem B, Schoppink L, Rotaru DC, Faiz A, Hendriks P, Mansvelder HD, van de Berg WD, Wouterlood FG (2014) Topographic mapping between basal forebrain cholinergic neurons and the medial prefrontal cortex in mice. J Neurosci 34:16234–16246.

Browning PG, Chakraborty S, Mitchell AS (2015) Evidence for mediodorsal thalamus and prefrontal cortex interactions during cognition in macaques. Cereb Cortex 25:4519–4534.

Card JP, Enquist LW (2014) Transneuronal circuit analysis with pseudorabies viruses. Curr Protoc Neurosci 68:1.5.1–1.5.39.

Card JP, Rinaman L, Lynn RB, Lee BH, Meade RP, Miselis RR, Enquist LW (1993) Pseudorabies virus infection of the rat central nervous system: ultrastructural characterization of viral replication, transport, and pathogenesis. J Neurosci 13:2515–2539.

Card JP, Levitt P, Enquist LW (1998) Different patterns of neuronal infection after intracerebral injection of two strains of pseudorabies virus. J Virol 72:4434–4441.

Cenquizca LA, Swanson LW (2007) Spatial organization of direct hippocampal field CA1 axonal projections to the rest of the cerebral cortex. Brain Res Rev 56:1–26.

Chen YH, Wu JL, Hu NY, Zhuang JP, Li WP, Zhang SR, Li XW, Yang JM, Gao TM (2021) Distinct projections from the infralimbic cortex exert opposing effects in modulating anxiety and fear. J Clin Invest 131: e145692.

Chiba AA, Kesner RP, Reynolds AM (1994) Memory for spatial location as a function of temporal lag in rats: role of hippocampus and medial prefrontal cortex. Behav Neural Biol 61:123–131.

Cholvin T, Loureiro M, Cassel R, Cosquer B, Herbeaux K, de Vasconcelos AP, Cassel JC (2016) Dorsal hippocampus and medial prefrontal cortex each contribute to the retrieval of a recent spatial memory in rats. Brain Struct Funct 221:91–102.

Chudasama Y, Robbins TW (2003) Dissociable contributions of the orbitofrontal and infralimbic cortex to pavlovian autoshaping and discrimination reversal learning: further evidence for the functional heterogeneity of the rodent frontal cortex. J Neurosci 23:8771–8780.

Chudasama Y, Robbins TW (2004) Dopaminergic modulation of visual attention and working memory in the rodent prefrontal cortex. Neuropsychopharmacology 29:1628–1636.

Chudasama Y, Robbins TW (2006) Functions of frontostriatal systems in cognition: comparative neuropsychopharmacological studies in rats, monkeys and humans. Biol Psychol 73:19–38.

Chudasama Y, Passetti F, Rhodes SE, Lopian D, Desai A, Robbins TW (2003) Dissociable aspects of performance on the 5-choice serial reaction time task following lesions of the dorsal anterior cingulate, infralimbic and orbitofrontal cortex in the rat: differential effects on selectivity, impulsivity and compulsivity. Behav Brain Res 146:105–119.

Chudasama Y, Nathwani F, Robbins TW (2005) D-Amphetamine remediates attentional performance in rats with dorsal prefrontal lesions. Behav Brain Res 158:97–107.

Chudasama Y, Doobay VM, Liu Y (2012) Hippocampal-prefrontal cortical circuit mediates inhibitory response control in the rat. J Neurosci 32:10915–10924.

Churchwell JC, Morris AM, Heurtelou NM, Kesner RP (2009) Interactions between the prefrontal cortex and amygdala during delay discounting and reversal. Behav Neurosci 123:1185–1196.

Das T, Ivleva EI, Wagner AD, Stark CE, Tamminga CA (2014) Loss of pattern separation performance in schizophrenia suggests dentate gyrus dysfunction. Schizophr Res 159:193–197.

Delatour B, Gisquet-Verrier P (2001) Involvement of the dorsal anterior cingulate cortex in temporal behavioral sequencing: subregional analysis of the medial prefrontal cortex in rat. Behav Brain Res 126:105–114.

Dowson JH, McLean A, Bazanis E, Toone B, Young S, Robbins TW, Sahakian BJ (2004) Impaired spatial working memory in adults with

attention-deficit/hyperactivity disorder: comparisons with performance in adults with borderline personality disorder and in control subjects. Acta Psychiatr Scand 110:45–54.

Dum RP, Levinthal DJ, Strick PL (2009) The spinothalamic system targets motor and sensory areas in the cerebral cortex of monkeys. J Neurosci 29:14223–14235.

Eagle DM, Baunez C, Hutcheson DM, Lehmann O, Shah AP, Robbins TW (2008) Stop-signal reaction-time task performance: role of prefrontal cortex and subthalamic nucleus. Cereb Cortex 18:178–188.

Fanselow MS, Dong HW (2010) Are the dorsal and ventral hippocampus functionally distinct structures? Neuron 65:7–19.

Gaykema RP, Luiten PG, Nyakas C, Traber J (1990) Cortical projection patterns of the medial septum-diagonal band complex. J Comp Neurol 293:103–124.

Ghashghaei HT, Hilgetag CC, Barbas H (2007) Sequence of information processing for emotions based on the anatomic dialogue between prefrontal cortex and amygdala. Neuroimage 34:905–923.

Harland B, Contreras M, Souder M, Fellous JM (2021) Dorsal CA1 hippocampal place cells form a multi-scale representation of megaspace. Curr Biol 31:2178–2190.e6.

Heidbreder CA, Groenewegen HJ (2003) The medial prefrontal cortex in the rat: evidence for a dorso-ventral distinction based upon functional and anatomical characteristics. Neurosci Biobehav Rev 27:555–579.

Hoover WB, Vertes RP (2007) Anatomical analysis of afferent projections to the medial prefrontal cortex in the rat. Brain Struct Funct 212:149–179.

Hunsaker MR, Rosenberg JS, Kesner RP (2008) The role of the dentate gyrus, CA3a,b, and CA3c for detecting spatial and environmental novelty. Hippocampus 18:1064–1073.

Ino T, Yasui Y, Itoh K, Nomura S, Akiguchi T, Kameyama M, Mizuno N (1987) Direct projections from Ammon's horn to the septum in the cat. Exp Brain Res 68:179–188.

Ishizuka N, Weber J, Amaral DG (1990) Organization of intrahippocampal projections originating from CA3 pyramidal cells in the rat. J Comp Neurol 295:580–623.

Jay TM, Witter MP (1991) Distribution of hippocampal CA1 and subicular efferents in the prefrontal cortex of the rat studied by means of anterograde transport of Phaseolus vulgaris-leucoagglutinin. J Comp Neurol 313:574–586.

Jones MW, Wilson MA (2005) Theta rhythms coordinate hippocampal-prefrontal interactions in a spatial memory task. PLoS Biol 3:e402.

Jones RS (1993) Entorhinal-hippocampal connections: a speculative view of their function. Trends Neurosci 16:58–64.

Kajiwara R, Wouterlood FG, Sah A, Boekel AJ, Baks-te Bulte LT, Witter MP (2008) Convergence of entorhinal and CA3 inputs onto pyramidal neurons and interneurons in hippocampal area CA1—an anatomical study in the rat. Hippocampus 18:266–280.

Kheirbek MA, Klemenhagen KC, Sahay A, Hen R (2012) Neurogenesis and generalization: a new approach to stratify and treat anxiety disorders. Nat Neurosci 15:1613–1620.

Kim H, Ährlund-Richter S, Wang X, Deisseroth K, Carlén M (2016) Prefrontal parvalbumin neurons in control of attention. Cell 164:208–218.

Kim WB, Cho JH (2017) Synaptic targeting of double-projecting ventral CA1 hippocampal neurons to the medial prefrontal cortex and basal amygdala. J Neurosci 37:4868–4882.

Krettek JE, Price JL (1977) Projections from the amygdaloid complex to the cerebral cortex and thalamus in the rat and cat. J Comp Neurol 172:687–722.

Kuramoto E, Pan S, Furuta T, Tanaka YR, Iwai H, Yamanaka A, Ohno S, Kaneko T, Goto T, Hioki H (2017) Individual mediodorsal thalamic neurons project to multiple areas of the rat prefrontal cortex: a single neuron-tracing study using virus vectors. J Comp Neurol 525:166–185.

Lee H, Wang C, Deshmukh SS, Knierim JJ (2015) Neural population evidence of functional heterogeneity along the CA3 transverse axis: pattern completion versus pattern separation. Neuron 87:1093–1105.

Li J, Liu T, Dong Y, Kondoh K, Lu Z (2019) Trans-synaptic neural circuit-tracing with neurotropic viruses. Neurosci Bull 35:909–920.

Li XG, Somogyi P, Ylinen A, Buzsáki G (1994) The hippocampal CA3 network: an *in vivo* intracellular labeling study. J Comp Neurol 339:181–208.

Lin X, Amalraj M, Blanton C, Avila B, Holmes TC, Nitz DA, Xu X (2021) Noncanonical projections to the hippocampal CA3 regulate spatial learning and memory by modulating the feedforward hippocampal trisynaptic pathway. PLoS Biol 19:e3001127.

Lu L, Igarashi KM, Witter MP, Moser EI, Moser MB (2015) Topography of place maps along the CA3-to-CA2 axis of the hippocampus. Neuron 87:1078–1092.

Luchicchi A, Mnie-Filali O, Terra H, Bruinsma B, de Kloet SF, Obermayer J, Heistek TS, de Haan R, de Kock CP, Deisseroth K, Pattij T, Mansvelder HD (2016) Sustained attentional states require distinct temporal involvement of the dorsal and ventral medial prefrontal cortex. Front Neural Circuits 10:70.

Malik R, Li Y, Schamiloglu S, Sohal VS (2022) Top-down control of hippocampal signal-to-noise by prefrontal long-range inhibition. Cell 185:1602–1617.e17.

Mar AC, Walker AL, Theobald DE, Eagle DM, Robbins TW (2011) Dissociable effects of lesions to orbitofrontal cortex subregions on impulsive choice in the rat. J Neurosci 31:6398–6404.

Marrone DF, Satvat E, Odintsova IV, Gheidi A (2014) Dissociation of spatial representations within hippocampal region CA3. Hippocampus 24:1417–1420.

McDonald AJ (1987) Organization of amygdaloid projections to the mediodorsal thalamus and prefrontal cortex: a fluorescence retrograde transport study in the rat. J Comp Neurol 262:46–58.

McDonald AJ (1991) Organization of amygdaloid projections to the prefrontal cortex and associated striatum in the rat. Neuroscience 44:1–14.

Montagrin A, Saiote C, Schiller D (2018) The social hippocampus. Hippocampus 28:672–679.

Moscarello JM, Maren S (2018) Flexibility in the face of fear: hippocampal-prefrontal regulation of fear and avoidance. Curr Opin Behav Sci 19:44–49.

Nakamura NH, Flasbeck V, Maingret N, Kitsukawa T, Sauvage MM (2013) Proximodistal segregation of nonspatial information in CA3: preferential recruitment of a proximal CA3-distal CA1 network in nonspatial recognition memory. J Neurosci 33:11506–11514.

O'Donnell P, Lavin A, Enquist LW, Grace AA, Card JP (1997) Interconnected parallel circuits between rat nucleus accumbens and thalamus revealed by retrograde transynaptic transport of pseudorabies virus. J Neurosci 17:2143–2167.

Passetti F, Chudasama Y, Robbins TW (2002) The frontal cortex of the rat and visual attentional performance: dissociable functions of distinct medial prefrontal subregions. Cereb Cortex 12:1254–1268.

Paxinos G, Watson C (2005) The rat brain in stereotaxic coordinates. Amsterdam: Elsevier Academic Press.

Petrovich GD, Canteras NS, Swanson LW (2001) Combinatorial amygdalar inputs to hippocampal domains and hypothalamic behavior systems. Brain Res Brain Res Rev 38:247–289.

Pitkänen A, Pikkarainen M, Nurminen N, Ylinen A (2000) Reciprocal connections between the amygdala and the hippocampal formation, perirhinal cortex, and postrhinal cortex in rat. A review. Ann N Y Acad Sci 911:369–391.

Prasad JA, Chudasama Y (2013) Viral tracing identifies parallel disynaptic pathways to the hippocampus. J Neurosci 33:8494–8503.

Prasad JA, Macgregor EM, Chudasama Y (2013) Lesions of the thalamic reuniens cause impulsive but not compulsive responses. Brain Struct Funct 218:85–96.

Ragozzino ME, Detrick S, Kesner RP (1999) Involvement of the prelimbic-infralimbic areas of the rodent prefrontal cortex in behavioral flexibility for place and response learning. J Neurosci 19:4585–4594.

Reppucci CJ, Petrovich GD (2016) Organization of connections between the amygdala, medial prefrontal cortex, and lateral hypothalamus: a single and double retrograde tracing study in rats. Brain Struct Funct 221:2937–2962.

Risold PY, Swanson LW (1997) Connections of the rat lateral septal complex. Brain Res Brain Res Rev 24:115–195.

Ropireddy D, Scorcioni R, Lasher B, Buzsáki G, Ascoli GA (2011) Axonal morphometry of hippocampal pyramidal neurons semi-automatically

reconstructed after *in vivo* labeling in different CA3 locations. Brain Struct Funct 216:1–15.
Rudebeck PH, Walton ME, Smyth AN, Bannerman DM, Rushworth MF (2006) Separate neural pathways process different decision costs. Nat Neurosci 9:1161–1168.
Ryu V, Watts AG, Xue B, Bartness TJ (2017) Bidirectional crosstalk between the sensory and sympathetic motor systems innervating brown and white adipose tissue in male Siberian hamsters. Am J Physiol Regul Integr Comp Physiol 312:R324–R337.
Saper CB (1985) Organization of cerebral cortical afferent systems in the rat. II. Hypothalamocortical projections. J Comp Neurol 237:21–46.
Sauer JF, Folschweiller S, Bartos M (2022) Topographically organized representation of space and context in the medial prefrontal cortex. Proc Natl Acad Sci U S A 119:e2117300119.
Shibata H (1993) Efferent projections from the anterior thalamic nuclei to the cingulate cortex in the rat. J Comp Neurol 330:533–542.
Shibata H, Kondo S, Naito J (2004) Organization of retrosplenial cortical projections to the anterior cingulate, motor, and prefrontal cortices in the rat. Neurosci Res 49:1–11.
Shimogawa Y, Sakuma Y, Yamanouchi K (2015) Efferent and afferent connections of the ventromedial hypothalamic nucleus determined by neural tracer analysis: implications for lordosis regulation in female rats. Neurosci Res 91:19–33.
Staiger JF, Nürnberger F (1991) The efferent connections of the lateral septal nucleus in the guinea pig: intrinsic connectivity of the septum and projections to other telencephalic areas. Cell Tissue Res 264:415–426.
Swanson LW (1981) A direct projection from Ammon's horn to prefrontal cortex in the rat. Brain Res 217:150–154.
Swanson LW, Cowan WM (1977) An autoradiographic study of the organization of the efferent connections of the hippocampal formation in the rat. J Comp Neurol 172:49–84.
Tamminga CA, Stan AD, Wagner AD (2010) The hippocampal formation in schizophrenia. Am J Psychiatry 167:1178–1193.
Vertes RP, Linley SB, Hoover WB (2015) Limbic circuitry of the midline thalamus. Neurosci Biobehav Rev 54:89–107.
Wang J, Barbas H (2018) Specificity of primate amygdalar pathways to hippocampus. J Neurosci 38:10019–10041.
Wang ME, Fraize NP, Yin L, Yuan RK, Petsagourakis D, Wann EG, Muzzio IA (2013) Differential roles of the dorsal and ventral hippocampus in predator odor contextual fear conditioning. Hippocampus 23:451–466.
Witter MP (1993) Organization of the entorhinal-hippocampal system: a review of current anatomical data. Hippocampus 3 Spec No:33–44.
Witter MP, Groenewegen HJ (1984) Laminar origin and septotemporal distribution of entorhinal and perirhinal projections to the hippocampus in the cat. J Comp Neurol 224:371–385.
Wittner L, Henze DA, Záborszky L, Buzsáki G (2007) Three-dimensional reconstruction of the axon arbor of a CA3 pyramidal cell recorded and filled *in vivo*. Brain Struct Funct 212:75–83.
Wouterlood FG, Saldana E, Witter MP (1990) Projection from the nucleus reuniens thalami to the hippocampal region: light and electron microscopic tracing study in the rat with the anterograde tracer Phaseolus vulgaris-leucoagglutinin. J Comp Neurol 296:179–203.
Ye X, Kapeller-Libermann D, Travaglia A, Inda MC, Alberini CM (2017) Direct dorsal hippocampal-prelimbic cortex connections strengthen fear memories. Nat Neurosci 20:52–61.
Zingg B, Chou XL, Zhang ZG, Mesik L, Liang F, Tao HW, Zhang LI (2017) AAV-mediated anterograde transsynaptic tagging: mapping corticocollicular input-defined neural pathways for defense behaviors. Neuron 93:33–47.
Zingg B, Peng B, Huang J, Tao HW, Zhang LI (2020) Synaptic specificity and application of anterograde transsynaptic AAV for probing neural circuitry. J Neurosci 40:3250–3267.